Thermochimica Acta 668 (2018) 142–151

Contents lists available at ScienceDirect

Thermochimica Acta

journal homepage: www.elsevier.com/locate/tca

A first-principles based description of the Hf-Ni system supported by high-temperature synchrotron experiments

A.J. Ross[a,*], T. Gheno[b], P.K. Ray[c], M.J. Kramer[c], X.L. Liu[a], G. Lindwall[d], B. Zhou[a], S.L. Shang[a], B. Gleeson[b], Z-K. Liu[a]

[a] Department of Materials Science and Engineering, The Pennsylvania State University, University Park, PA 16802, USA
[b] Department of Mechanical Engineering & Materials Science, University of Pittsburgh, Pittsburgh, PA 15261, USA
[c] Ames Laboratory, US-DOE, Ames, IA 50011, USA
[d] Department of Materials Science and Engineering, KTH Royal Institute of Technology, Brinellvägen 23, SE-11428 Stockholm, Sweden

A B S T R A C T

Hf-Ni is an important binary system for high temperature alloys and shape memory alloys which has been investigated several times in the literature but often using samples of Hf contaminated by Zr. The thermodynamics of this system are remodeled in this work based on first-principles calculations and additional experiments using Hf with relatively low Zr contamination (0.25 wt. %). Diffusion couples in the Ni-rich portion of the Hf-Ni system heat treated at 1173, 1273 and 1373 K are used to measure phase stability and Hf solubility in the fcc phase. The solubility observed in fcc Ni from $Ni/Ni_{50}Hf_{50}$ (at.%) diffusion couples is larger than that observed in previous experiments. These results are the only source fit to during modeling of the fcc solubility to mitigate effects from Zr contamination. Data in the literature suggests that the high temperature crystal structure of the B33 NiHf phase is, in fact, the B2 structure. High temperature synchrotron measurements provide confirmation of this crystal structure. Modeling of the B2 phase was aided by first-principles calculations using special quasi-random structures (SQS). The present CALPHAD model will prove useful when designing shape memory alloys containing Hf and when modeling the Hf activity in Ni-base high temperature alloys.

1. Introduction

The Hf-Ni system is of key importance to high temperature oxidation resistant alloys where Hf has been observed to reduce the growth rate of protective oxides and improve scale adherence [1]. In MCrAlX overlay coatings (M = Ni, Co or Fe and X = Y,Hf,Zr, or La), platinum diffusion aluminides (e.g. MDC-151 L) and Ni-base superalloys (e.g. Rene N5), Hf has proven to be especially beneficial in providing oxidation resistance. These materials are based on the following phases: fcc solid solution, γ'-Ni_3Al ($L1_2$) and β-NiAl (B2). Both the $L1_2$ phase the B2 phase are rich in Al, making them important for forming a protective oxide layer of α -Al_2O_3 during oxidation. The disordered fcc phase will often be in equilibrium with the $L1_2$ or the B2 phase in MCrAlX coatings. Hence, it is important to understand the solubility and activity of Hf in the disordered phase. It is also especially important to consider the stability of the B2 phase in the Hf-Ni system since the thermodynamics from this binary system will play an important role in the reactivity of Hf during oxidation of the β -NiAl phase.

Hf-Ni is also considered an important binary system for shape memory applications. The Ti-Hf-Ni system has been long considered a rich source of shape memory compositions due to the relative low cost of these alloys [2]. The large stability range of the B2-NiTi phase plays a role in the design of these alloys. It has been suggested that NiTi forms a complete solid solution with NiHf at high temperatures but the high temperature phase rich in Hf could not be analyzed after quenching [3]. Although it is likely that this phase has a B2 structure, no experiments have directly confirmed this. Confirmation of this phase structure will offer justification to thermodynamic models which describe it as the B2 phase. Finally the Hf-Ni system is important to consider due to the strong stability of $NiXHf_2$ Heusler and NiXHf half Heusler phases for several alloying elements X and because of the eutectics often present in those Hf-Ni-X systems [4–6].

The Hf-Ni system has been modeled several times in the literature. It was recently modeled by Wang et al. [7] using new experimental diffusion couples. Then, the system was re-modeled by Zhang et al. [8] in an investigation of the Ni-rich part of the Al-Hf-Ni system. Finally a first-principles based assessment was carried out by Berche et al. [6] with little focus on experiments. Unfortunately, many thermochemical experiments in the literature used by Wang et al used Hf with ~2-3 wt. % Zr. This is not ideal for equilibrium measurements and phase boundary measurements as Zr may alter the phase boundary of the system or stabilize a phase which would not have otherwise been present. Although it is not wise to discard these equilibria measurements entirely, some uncertainty must be attributed to the position of phase boundaries – especially for the equilibrium between the fcc solution phase and Ni_5Hf which will have a large impact on the resulting activity

* Corresponding author.
E-mail address: austinross42@gmail.com (A.J. Ross).

https://doi.org/10.1016/j.tca.2018.08.011
Received 24 May 2018; Received in revised form 3 August 2018; Accepted 11 August 2018
Available online 17 August 2018
0040-6031/

of Hf. While not all experimental data in the literature reports the presence of Zr in their Hf samples, it is seems likely that Zr contamination is more probable in older experiments given the cost in detecting and removing Zr from Hf [9].

The present theoretical and experimental work seeks to expand (1) the previously investigated first-principles in this system, (2) the phase stability and solubility of Hf in this system using high purity Hf, and (3) the high temperature stability of the NiHf phase. Finite temperature, first-principles calculations are carried out on select Ni-rich intermetallic phases to obtain Gibbs energies for each of these phases. Special quasi-random structures (SQS) calculations were performed to obtain enthalpies of mixing in the fcc, bcc and B2 phases. This information is implemented in the computation of phase diagrams (CALPHAD) remodeling of this system. Diffusion couple experiments are used to confirm the stability of the Hf_3Ni_7 phase. These experiments confirm that there is a larger solubility of Hf in fcc compared to previous experiments. First-principles calculations of the B33-NiHf and B2 phases shows the expected results that the B2 phase is mechanically stable and has a higher calculated molar entropy compared to the B33 phase. This suggests the possibility of B2 being the high temperature stable phase. Differential scanning calorimetry (DSC) is used to measure the transition temperature of the high temperature phase and high temperature synchrotron experiments performed on a Ni-50Hf (at.%) alloy confirms the presence of the B2 phase. This work is part of a larger investigation of the Al-Cr-Hf-Ni system.

2. Literature review

Although the Hf-Ni system has been investigated many times, results often came with the presence of Zr impurities in the Hf used. For instance, investigations into equilibria in this system by Hajjaji et al. [10], Svechnikov et al. [11] Bsenko et al. [12] contained ~2.5, ~0.65, and ~3 wt.% Zr in the starting Hf alloys, respectively. Investigations into the formation enthalpies of intermetallic compounds by Selhaoui et al. [13] and Bencze [14], contained ~2.3 and ~2.52 wt.% Zr, respectively, in the starting Hf alloys. An additional complicating factor is that Hf has a very high solubility for O [15] which is only briefly addressed by Guo et al. [16,17]. The most recent collection of the literature in this system are included in the thermodynamic re-modeling by Wang et al. [7]. While many sources are listed, the details of these experiments are not fully summarized. What follows is an in-depth discussion of this literature and more recent experiments in this system.

2.1. Equilibria

The Ni-rich part of the Hf-Ni system (65–80 at. % Ni) has been investigated by Bsenko et al. [12] using x-ray diffraction (XRD) to study equilibria in samples heat treated at 1173 to 1593 K. Differential thermal analysis (DTA) of arc-melted samples was also used to tabulate the invariant reactions within this composition range. Svechnikov et al. [11] and Yeremenko et al. [18] both used DTA to measure the liquidus of the system from 0 to 100 and 0 to 50 at.% Ni, respectively. Yeremenko et al. [18] reported performing additional equilibria measurements at 1473 K, 1373 K and 1273 K, but only data at 1375 K is reported.

Wang performed diffusion couple experiments at 1123 and 1173 K for 1440 and 1200 h, respectively. Electron probe micro-analysis (EPMA) was used to measure the Hf solubility in fcc-Ni, the Ni solubility in hcp-Hf, and the composition range of the $NiHf_2$ phase. Hajjaji et al. [10] also studied the solubility of Hf in fcc-Ni using XRD and transmission electron microscopy (TEM) in the temperature range of 773–1373 K. Notably, heat treatment times for measurements in this study were unspecified except at 1333 K with a heat treatment time of 24 h.

2.2. Thermochemical data

Experiments by Bencze [14] using Knudsen effusion cell spectrometry represents the most extensive investigation of the thermochemical information of the solid phases in the Hf-Ni system. This data set includes Gibbs energies of formation, enthalpies of formation, associated activities and, to a lesser extent, phase stabilities at 1418 and 1473 K. Selhaoui et al. [13] and Guo et al. [16,17], both measured formation enthalpies of compounds via direct synthesis calorimetry for a range of temperatures between 1323 K and 1623 K and at 1477 K, respectively.

The most recent thermochemical investigation into the liquid phase was carried out by Popoprigora et al. [19,20], on Hf-Ni melts at 1770 ± 5 K using calorimetry. Earlier calorimetry measurements were also carried out by Selhaoui et al. [13] at 1473 and 1633 K, and by Sudavtsova and Sharkina [21] at 1877 K.

2.3. First-principles data

The formation enthalpy of the known compounds in the binary system was investigated by Berche [6] in a larger investigation of the Hf-Ni-Sn system. Calculations were performed in the Vienna ab initio simulation package (vasp) [22] using settings intended to attain reasonable accuracy for values of the compound formation enthalpy. However, this study did not investigate the B2 phase or the $L1_2$ phase and did not include enthalpies for the disordered fcc-A1 and bcc-A2 solution phases. Additional sources of compound formation enthalpies for select compounds are also available from high-throughput DFT calculations such as work using AFLOW [23].

2.4. Experimental evidence of the B2 phase

In the investigation by Wang et al. [7] the high temperature allotrope of NiHf is not explicitly identified as the B2 phase. This is largely due to the fact that there has been no direct observation of this phase in the literature. Experiments performed by Yeremenko et al. [18] in the Hf-Ni-Ti system suggests a complete solid solution between β -NiTi and the high temperature NiHf phase through phase relations of quenched alloys and DTA measurements. However it was not possible for Yeremenko et al. [18] to quench this phase from high temperature and only the low temperature B33 allotrope was ever resolved during experiments. There are also other experiments by Eremenko et al. [24] which studied solid solutions between NiZr and NiHf. A complete solid solution was observed for the B33 phase at low temperatures and a large solution range for a high temperature phase of B2 was also suggested but was again too difficult to resolve from quenching [24].

2.5. Non-stoichiometric compounds

As stated before, Wang et al. [7] observed an appreciable composition range in the Hf_2Ni phase. A small composition range (0.3 at. %) was also observed in Hf_2Ni_7. Several other ternary investigations have noted significant solubility in this phase. Experiments by Nash and West [25,26], Khorunov et al. [5], and Zhang et al. [8] all observed that tielines consistent with a Hf_2Ni_7 phase which could dissolve a significant amount of Ni. In this work, a model for this phase is adopted from our larger investigation into the Al-Cr-Hf-Ni system and a suggested solubility is added based on modeling in the ternary Al-Hf-Ni system.

3. Thermodynamic models

3.1. Stoichiometric intermetallic phases

For a stoichiometric compound Hf_ANi_B, the molar Gibbs energy of this phase, $G_m^{Hf_ANi_B}$, can be given as:

$$G_m^{Hf_A Ni_B} - \left(\frac{A}{A+B}\right)H_{Hf}^{SER} - \left(\frac{A}{A+B}\right)H_{Ni}^{SER} = a + bT + cT\ln T + dT^2 + \frac{e}{T} + fT^3$$

where a through are constants and H_i^{SER} is the enthalpy of element i in the standard element reference state. When experiments are not available to fit these parameters they can instead be determined using first-principles calculations [27]. However, this is not always considered necessary and in some cases a simpler Kopp–Neumann type approach is used [28]. In such cases the Gibbs energy is given as:

$$G_m^{Hf_A Ni_B} - \left(\frac{A}{A+B}\right)H_{Hf}^{SER} - \left(\frac{A}{A+B}\right)H_{Ni}^{SER} = \left(\frac{A}{A+B}\right)G_m^{Hf} + \left(\frac{B}{A+B}\right)G_m^{Ni} + A^{Hf_A Ni_B} - B^{Hf_A Ni_B}T$$

Where $A^{Hf_A Ni_B}$ and $B^{Hf_A Ni_B}$ are values used to fit the available formation enthalpy and entropy, respectively, and the heat capacity is given by the mechanical mixture of the individual elements. Both models are used in this work.

3.2. Solution phases

The bcc, fcc, hcp and liquid phases are modeled using the compound energy formalism [29] (CEF), with mixing on a single symmetry equivalent sublattice. For each of the solid solution phases the sublattice is occupied by both Ni and Hf with sublattice model $(Ni,Hf)_a(Va)_b$ where a and b represent the relative stoichiometry for lattice sites and modeled interstitial sites, respectively. Mixing occurs between end-members - those compounds representing extremes in sublattice occupation: Ni_aVa_b and Hf_aVa_b. The Gibbs energy of the solution phase is constructed using contributions from the mechanical mixing of these end-members, configurational entropy and an excess term. The excess Gibbs energy, G_m^{ex} is considered using a Redlich-Kister polynomial:

$$G_m^{ex} = \sum_i \sum_{j>i} x_i x_j \sum_\nu {}^\nu L_{i,j}(x_i - x_j)^\nu$$

Where ${}^\nu L_{i,j}$ is the ν th order interaction parameter between species i and j expanded out in mole fraction of these components: x_i and x_j respectively. In this work the interaction parameters are expanded to the first order of T: ${}^\nu L_{i,j} = {}^\nu A_{i,j} + {}^\nu B_{i,j}T$ Where ${}^\nu A_{i,j}$ is used to fit to the excess enthalpy and ${}^\nu B_{i,j}$ the excess entropy for a given phase.

3.3. Non-stoichiometric intermetallic phases

Wang et al. [7] observed significant solubility in the Ni_1Hf_2 phase and thus modeled this phase using the sublattice model $(Ni,Hf)_1Hf_2$ with the assumption that Ni could dissolve further Hf. This model is adopted in this work with Ni_1Hf_2 and Hf_1Hf_2 end-members adjusted using first-principles calculations. Aside from this, the model is the same as the one found by Wang et al. [7]. The Ni_7Hf_2 phase is modeled using the sublattice model: $(Ni)_7(Hf,Ni)_2$. This model was chosen in this work to account for Hf solubility observed in higher order systems [25,26], of the Al-Cr-Hf-Ni system.

3.4. The order disorder model

The order disorder model in this work describes the bcc-A2 to B2 and fcc-A1 to $L1_2$ transformations. $L1_2$ is not stable in the binary but it is still important to model this phase for higher order systems where it is stable - such as the Ni-Al-Hf system [30]. The model used in this work to describe these transformations is the one developed by Ansara [31] and Dupin [32]. While a more physical version of this model uses four sublattices, this paper will use the two sublattice (2SL) model for both the B2 and $L1_2$ ordered phases given the wide-spread application of the 2SL model. For a given disordered phase Θ and its corresponding ordered phase Θ', the 2SL model treats the Gibbs energy of the ordered phase, $G_m^{\Theta'}$, as a sum the Gibbs energy of the disordered solution phase, G_m^{Θ}, and an ordering contribution, $\Delta G_m^{\Theta'}$.The full form of the ordering contribution can be found elsewhere and will not be discussed here [33,34].

The interactions and end-members of the ordered energy contribution are modeled using the concept of bond energies between elements i and j, $U_{i,j}$, on a given sublattice. For the Hf-Ni system there are three ordered compounds considered in the 2SL model. The Gibbs energy of these compounds is given as:

$$G_{HfNi_3} = 3U_{HfNi} + \alpha_{HfNi_3}$$

$$G_{Hf_2Ni_2} = 4U_{HfNi}$$

$$G_{Hf_3Ni} = 3U_{HfNi} + \alpha_{Hf_3Ni}$$

Where the α terms represent changes in the bonding environment between each compound [35]. U_{HfNi} and the α terms are used to fit to available thermochemical and phase equilibria data in the same way that interaction parameters are:

$$U_{HfNi} = A_U^{HfNi} + B_U^{HfNi}T$$

And

$$\alpha_i = A_i + B_i T$$

In the 4SL model there is an equivalency between sublattice configurations due to the symmetry between Wyckoff sites in the $L1_2$ phase and B2 phase. This results in equivalency between end-members of the 4SL model, e.g.: $G_{i:j:j:j} = G_{j:i:j:j} = G_{j:j:i:j} = G_{j:j:j:i}$, and interactions in the 4SL model, e.g.: $L_{i,j:j:j} = L_{j:i,j:j:j} = L_{j:j:i,j:j} = L_{j:j:j:i,j}$. Since the 2SL model represents a simplification of the more complex 4SL model, modifications to the energy surface of the 2SL model are made through relations in the interaction parameters to account for this equivalency. The full form of these relations can be found elsewhere [34].

4. First-principles methodologies

4.1. Finite temperature calculations

Although first-principles calculation have already been carried out by Berch et al. [6] it is of interest to calculate the finite temperature properties of the B2 phase, the low temperature HfNi allotrope and the high temperature compound $NiHf_2$. The $NiHf_2$ is of interest since it will come in equilibrium with the B2 phase at high temperatures. All calculations are carried out in the Vienna ab initio software package [22] (vasp 5.3.3) using the projector augmented wave (PAW) method and a planewave cut-off of 400 eV. Electronic exchange and correlation is described using the generalized gradient approximation via the implementation by Perdew, Burke, and Ernzerhof [36] (PBE). The recommended PAW potentials by vasp for Hf and Ni are used in this work [37]. Brillouin zone integration was carried out using the tetrahedron-bloch method with the fully automatic function of k-mesh generation provided by vasp. A length of 80 was provided for all calculations within this method [37]. This kpoint method results in a variable kpoint per reciprocal atom (kppra) value but the smallest kppra was 5000 which results in acceptable accuracy.

Finite temperature information is obtained using the approach detailed by Shang and Wang [38,39], where the Helmholtz free energy, $F(V, T)$, is taken as the sum of the 0 K energy, E^{0K}, the vibrational Helmholtz free energy, $F_{vib}(V, T)$, and the thermal-electronic Helmholtz free energy, $F_{T-ele}(V, T)$. In this work $F_{vib}(V, T)$ is obtained with the quasi-harmonic Debye model as described by Shang et al. [38] where a Debye temperature, $\Theta(V, T)$, is calculated using structures at different volumes to obtain the energy as a function of volume, $E^{0K}(V)$, through a four parameter Birch-Murnaghan equation of state fitting. A scaling factor for $\Theta(V, T)$ to account for the crystal anisotropy of a given phase was calculated using the methods described by Shang et al. [40].

4.2. SQS calculations

SQS calculations are carried out in vasp using the setting described above. bcc-A2 mixing enthalpies were calculated using binary structures developed by Jiang et al. [41]. fcc-A1 mixing was calculated using structures developed by Wolverton et al. [42] and B2 mixing was calculated using structures developed by Jiang et al. [43]. All calculations followed a three-tiered relaxation scheme during vasp structure calculations: 1st only volume was allowed to relax, 2nd volume and shape were allowed to relax, and 3rd volume, shape and ion position were allowed to relax. Mixing enthalpies were only kept if the corresponding structure kept its crystal symmetry. This was tested using radial distribution functions to assess the symmetry of the structures.

5. Experimental methodologies

The experiments were performed using a HfNi ingot of nominally equiatomic composition, $Hf_{50}Ni_{50}$ (at. %), received from the Materials Preparation Center of Ames Laboratory [44]. The Hf contained 0.25 wt. % Zr. The ingot was made by argon arc melting, drop cast into a 10 mm diameter rod, and homogenized for 6 h at 1473 K plus 48 h at 1423 K in vacuum. The homogenization was part of a standard treatment to achieve compositional and microstructural stability for subsequent testing outside the scope of this study.

5.1. Diffusion couple

Diffusion couples were made between the HfNi alloy and pure Ni in order to study phase equilibria in the Ni-rich half of the HfNi system. The Ni specimens were taken from a high purity (99.999%), 1 mm thick plate received from Goodfellow. Specimens of dimensions 4 × 4 × 1 mm were ground using SiC papers, polished with diamond suspensions down to a 3 μm finish, and ultrasonically cleaned in ethanol. Couples were made by placing Ni and HfNi specimens in a silicon nitride clamping device, using Al_2O_3 powder to keep the samples leveled, and heat treating the assembly 30 min at 1373 K (1173 K couple) or 1 h at 1423 K (other couples) in laboratory air. After slow cooling, the couples were vacuum-encapsulated in quartz capsules and annealed at 1173, 1283 and 1373 K for 500, 190, and 100 h, respectively. The diffusion heat treatments were terminated by water quenching.

Polished sections of the heat-treated couples were prepared by standard metallographic procedures. Composition profiles were measured by electron probe micro-analysis (EPMA) using a JEOL JXA-8530F field emission gun instrument. The measured intensities were converted to concentrations via a built-in ZAF calibration procedure, using Hf and Ni as standards. A step size of 5 μm was used for overall scans of the diffusion regions, and 1 μm steps were used for detailed scans of the Ni/$HfNi_5$ interface region.

5.2. In-situ observation of phase transition

The high temperature phase transformation was observed using Differential Scanning Calorimetry (DSC) and time-resolved synchrotron based High Energy X-Ray Diffraction (HEXRD). The DSC experiments were performed using a NETZSCH 2000 calorimeter, in inert ultra-high purity argon environment. The sample was heated from room temperature to 1400 °C and then cooled back to room temperature at a rate of 10 °C/min. The time-resolved HEXRD experiments were carried out at the Advanced Photon Source (APS) at Argonne National Laboratory, in sector 11, beamline ID-11-C (energy – 105.6 keV, wavelength – 0.118 Å). The samples were prepared by sectioning the cast HfNi alloys and thinning down the sections to ~500 μm. The samples were then stacked in a Linkham TS1500 resistance furnace. These samples were then heated to 1490 K using an initial heating rate of 30 K/min till 1373 K and 10 K/min from 1373 to 1490 K. The diffraction data was collected using a Perkin-Elmer detector.

Table 1
Calculated entropies at 298.15 K, $S^{298.15}$, and enthalpies of formation at 298.15 K, $\Delta H^{298.15K}$. Comparison is made to calculated values by Berche et al. [6].

Phase	Volume	ΔH (kJ/mole-atom)	ΔH [6] (kJ/mole-atom)	$S^{298.15}$ (J/mole-atom·K)
Ni (fcc-A1)		0	–	–
Ni5Hf (C15b)		−33.67	−33.65	27.4825
Ni7Hf2		−45.18	−45.10	–
Ni7Hf3		−48.88	−48.71	–
NiHf (B33)		−50.00	−50.06	38.8575
NiHf (B2)		−41.77	–	40.29
NiHf2		−32.88	−32.85	51.5817
Hf (fcc-A1)		6.92	–	–
Hf (hcp-A3)		0	0	38.8683
Ni_3Hf ($L1_2$)		−51.41	–	29.0286
$NiHf_3$ ($L1_2$)		−1.60	–	–

6. Results and discussion

6.1. Results from first-principles

A list of calculated enthalpies formation at 298.15 K, $\Delta H^{298.15K}$ and entropies at 298.15 K, $S^{298.15}$, are given in Table 1. Data by Berche [6] is given for comparison. Formation enthalpies from Berche agree well with the present calculated values. The entropy at 298.15 K for the NiHf B2 phase is higher than the entropy for the B33-NiHf phase while the formation enthalpy for the B2 phase is higher than that of the B33 phase. This is the expected behaviour for the thermodynamics of high-temperature and low temperature phases. The difference in the formation enthalpy is around 8 kJ, however, and it is difficult to ascertain directly from first-principles if this is surmountable for the B2 phase based on the entropy difference between these two phases and the accuracy of the present vibrational calculations.

Calculated mixing enthalpies for the fcc, bcc and B2 solutions are presented in Table 2. Also included are the formation enthalpies of the ordered B2 and $L1_2$ compounds with respect to their respective disordered solutions. Mixing was more positive for dilute Hf-rich calculations compared to dilute Ni-rich calculations. There is a sign change between the two extremes in composition in the fcc phase. This is most likely caused by the size mismatch between each element. This may explain why the sign does not flip on the bcc portion of the diagram - since the bcc Hf phase has a greater equilibrium volume than the fcc phase and can therefore accommodate more strain in the lattice. The ordering contributions are much more negative compared to the disordered solutions, as expected.

6.2. Diffusion couple experimental results

The phases present after annealing of the diffusion couples, identified from the composition profiles, are summarized in Table 3 (partial

Table 2
Calculated enthalpies of mixing for the fcc-A1, bcc-A2, and B2 solutions.

	ΔH (kJ/mole-atom)		ΔH (kJ/mole-atom)
$Ni_{32}Hf_1$ (bcc-A2)	−9.13	$Ni_{32}Hf_1$ (fcc-A1)	−6.75
$Ni_{0.75}Hf_{0.25}$ (bcc-A2)	−17.06	$Ni_{0.75}Hf_{0.25}$ (fcc-A1)	−6.45
$Ni_{0.5}Hf_{0.5}$ (bcc-A2)	−8.81	$Ni_{0.5}Hf_{0.5}$ (fcc-A1)	−6.46
$Ni_{0.25}Hf_{0.75}$ (bcc-A2)	−8.06	$Ni_{0.25}Hf_{0.75}$ (fcc-A1)	3.65
Ni_1Hf_{32} (bcc-A2)	−1.30	Ni_1Hf_{32} (fcc-A1)	2.24
NiHf (B2)	−55.15	Ni_3Hf ($L1_2$)	−49.68
$Ni_{0.5}(Hf_{0.5}Ni_{0.5})_{0.5}$ (bcc-B2)	−29.94	$NiHf_3$ ($L1_2$)	3.59
$Hf_{0.5}(Hf_{0.5}Ni_{0.5})_{0.5}$ (bcc-B2)	−10.22		

Table 3
Phases of the Ni-rich half of the HfNi system observed after annealing of the Ni/HfNi diffusion couples. Phases observed in these experiments are marked "x".

T (K)	1123 [7]	1173 [7]	1173[present]	1373[present]
Ni	x	x	x	x
$HfNi_5$	x	x	x	x
Hf_2Ni_7	x	x	x	x
$HfNi_3$	x	x	x	x
Hf_3Ni_7				x
Hf_7Ni_{10}	x	x	x	x
Hf_9Ni_{11}	x	x	x	x
HfNi	x	x	x	x

oxidation of the 1283 K couple prevented reliable identification of the complete sequence at that temperature). Micrographs and composition profiles obtained from the 1173 K couple are given in Fig. 1 as an example. This information is compared to diffusion couple work by Wang et al. [7] in the same table. Phase observations are in good agreement. The results are also in good agreement with ternary diffusion couple experiments at 1173 K in the Hf-Ni-Ti system in which the same phases are observed near the Hf-Ni system [45]. Detailed analysis of the Ni/$HfNi_5$ interface region allowed the Hf solubility in γ-Ni to be determined; the measured values are plotted in Fig. 8a and will be discussed later.

6.3. High temperature experimental results

The differential scanning calorimetry (DSC) thermogram is shown in Fig. 2a. Interestingly, the exothermic peak corresponding to the phase transformation at 1433 K exhibits a significant asymmetry. Similarly, during cooling, one can observe a pronounced asymmetry. This is suggestive of a two-step transformation process (similar to the phase transformations in the TiAlNb system [47]). The temperature-dependent high energy x-ray diffraction (HEXRD) pattern is shown n Fig. 2b, with the powder diffraction pattern from the low temperature HfNi phase superimposed. The data is represented in a 2D plot, with the lines indicating the location of Bragg peaks in Q-space. The peak colors indicate the intensity of the peaks. Therefore, the phase transformation is indicated by the appearance of new peaks at approximately 1433 K, as indicated in Fig. 2b. There is a good agreement on the transformation temperatures (~1433 K) between the DSC measurements and the temperature-dependent diffraction data. It should be noted that the transformation, as observed in the HEXRD data is not a military type transformation and is constrained by kinetics. The peak intensities of the room temperature phase decreases but doesn't disappear completely. This indicates that the transformation kinetics are still sluggish and the transformation, during the synchrotron experiments, did not go to completion. In fact, the initial intensities during the appearance of the B2 phase at 1433 K is rather weak, with the intensities becoming significantly higher around 1458 K. Upon careful examination of the diffraction data, the B2 peaks first appear at temperatures a few degrees lower than 1433 K (corresponding to the pre-peak in the DSC thermogram in Fig. 2a) and gain in intensity beyond this temperature.

Similar phase transformations have been investigated in the Ti-Al-Nb system [46]. The phase section was predicted on the basis of subgroup selections while cooling from high temperatures (as opposed to heating). The B2 phase in the Ti-Al-Nb system was predicted to transform initially to a B19 phase (Pmma) and eventually to the Cmcm phase [46]. We report the phase transformation during heating, with the room temperature Cmcm phase transforming to a B2 structure at elevated temperatures. The asymmetry and splitting n the DSC peak could be an indicator of a deeper underlying transformation mechanism that we do not yet understand completely and was not captured in the HEXRD data due to inadequate time resolution and relatively higher heating rates.

6.4. Results from CALPHAD optimization

CALPHAD optimization was done using the Parrot module of Therm-Calc [47]. The model parameters were first adjusted using

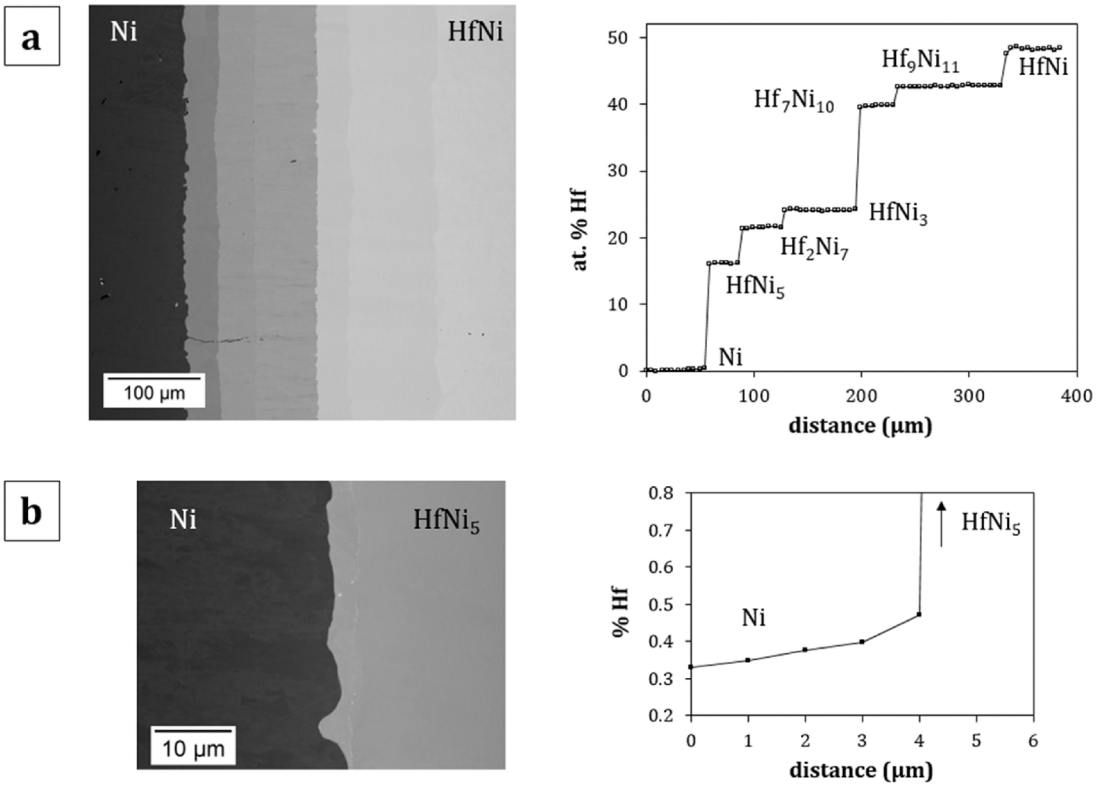

Fig. 1. Micrograph and composition profile obtained from Ni/HfNi diffusion couple annealed 500 h at 1173 K. (a): overview; (b): detailed analysis of the Ni/$HfNi_5$ interface region.

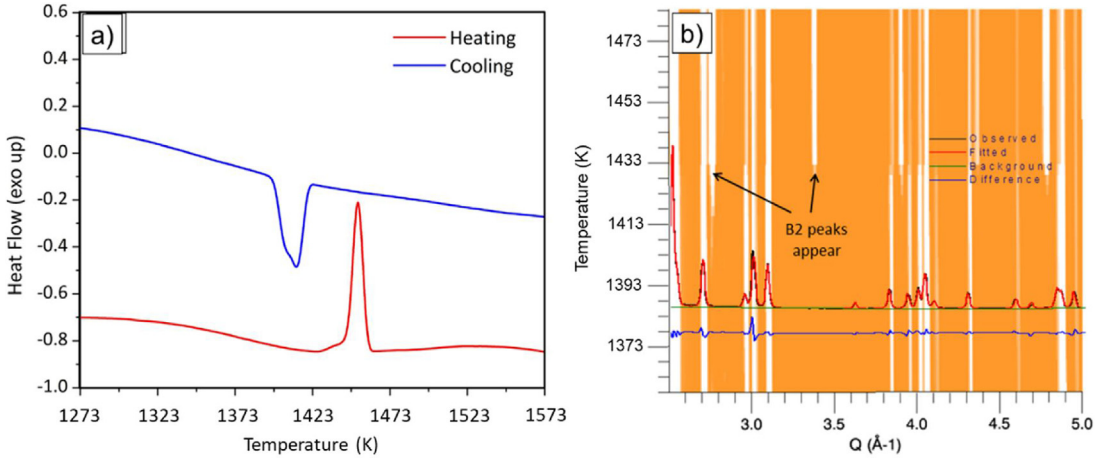

Fig. 2. (a) DSC thermogram of the equiatomic Hf-Ni alloy, plotted from data collected during heating and cooling at 10 K/min; (b) temperature-dependent diffractogram plotted from the HEXRD data. The vertical lines indicate the Bragg peaks in Q-space, while the line colors indicate the peak intensities. A powder pattern of the low temperature HfNi is superimposed on the HEXRD plot in order to accentuate the appearance of the peaks corresponding to the B2 phase.

thermochemical data from the first-principles calculations. Following this, the parameters were adjusted using both first-principles and experimental data. The resulting parameters and thermodynamic database can be found in the supplementary materials section.

6.4.1. Intermetallic stability

A plot of the formation enthalpies calculated from the present model at 1413.15 K and 298.15 K compared to experimentally determined enthalpies of formation and calculated enthalpies of formation is given in Fig. 3. Data by Benscze et al. [14] at 1413 K is not fully reproduced at this temperature. This is due to a closer fit to first-principles data in this work in the fcc phase and the result of fitting to the available invariant reactions and liquidus information. Only two compounds fall on the convex hull according to DFT: B33-NiHf and Ni_3Hf (R-3 m). In the present modeling, these phases are also the only ones present on the convex hull at 298.15. However, C15b-Ni_5Hf is stabilized at 302 K and this phase is so close to the convex hull as to be practically stable at low temperatures in the present predictions.

Calculated molar entropies from the present modeling for the Ni3Hf (L12), B33, B2, C16, and C15b phases is given in Fig. 4 compared to values obtained from first-principles calculations. Calculated trends in entropy are replicated in the present model but the magnitude of entropy was not. The C15b phase required a higher entropy to match observed invariant equilibria with the liquid and the C16 phase required a decrease of ~10 J/mol-atom-K at 298.15 K. The entropy difference between B33 and B2 modeled in this work was much larger compared to the value calculated from first-principles. Although it is possible that this is related to uncertainty in the equilibria near this phase, it is more likely caused by sources of error in the bonding described between B33 and B2 through the PBE, PAW potentials.

Ni activities measured by Bencze [14] compared to the calculated activities in the present database are shown in Fig. 5. Good agreement is

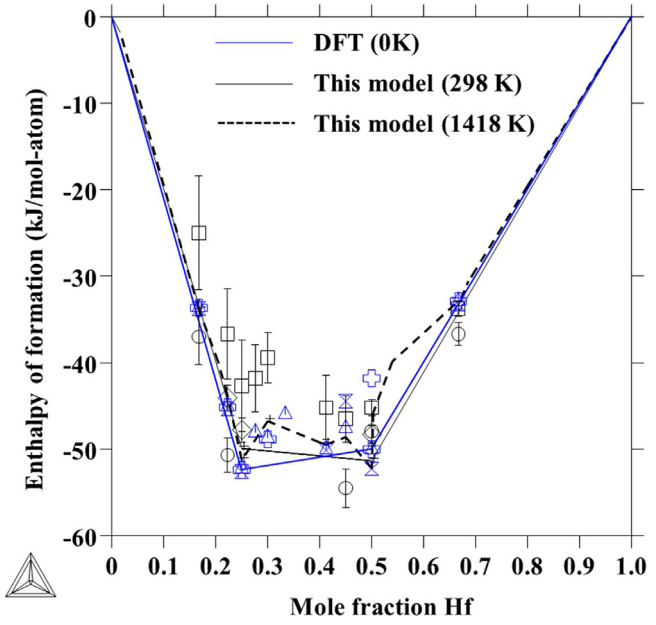

Fig. 3. Formation enthalpy of compounds at 0 K by first-principles and at 298 and 1418 K as calculated from the present model. Comparison is made to experiments with reported error bars by at 1418 K by Bencze [14] (□), 1477 K by Guo [16,17], (◇), and at 1323 K by Selhaoui [51] (○) and first-principles calculations at 0 K in this work (✚), and by Berche [6] (△) and Curtarolo [23] (⊠).

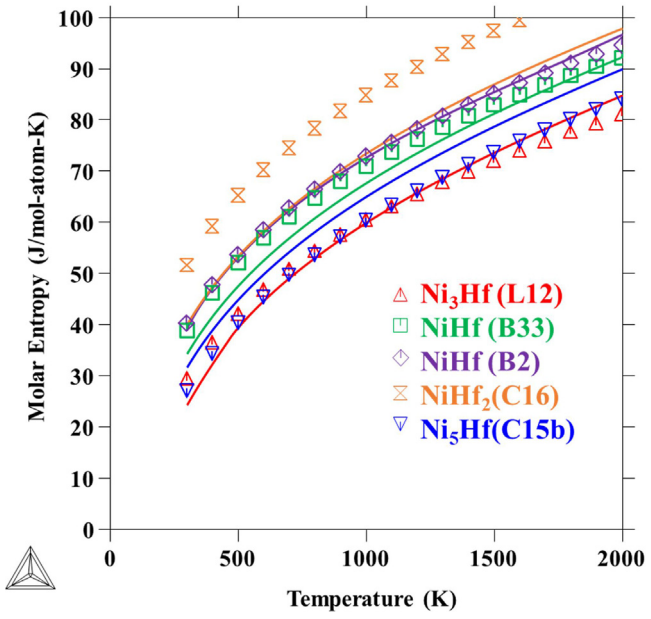

Fig. 4. Calculated molar entropy for the compounds Ni3Hf ($L1_2$), NiHf (B33), NiHf (B2), NiHf2 (C16), and Ni5Hf (C15b) (solid lines) and calculated molar entropies for compounds from first-principles, finite temperature calculations (symbols).

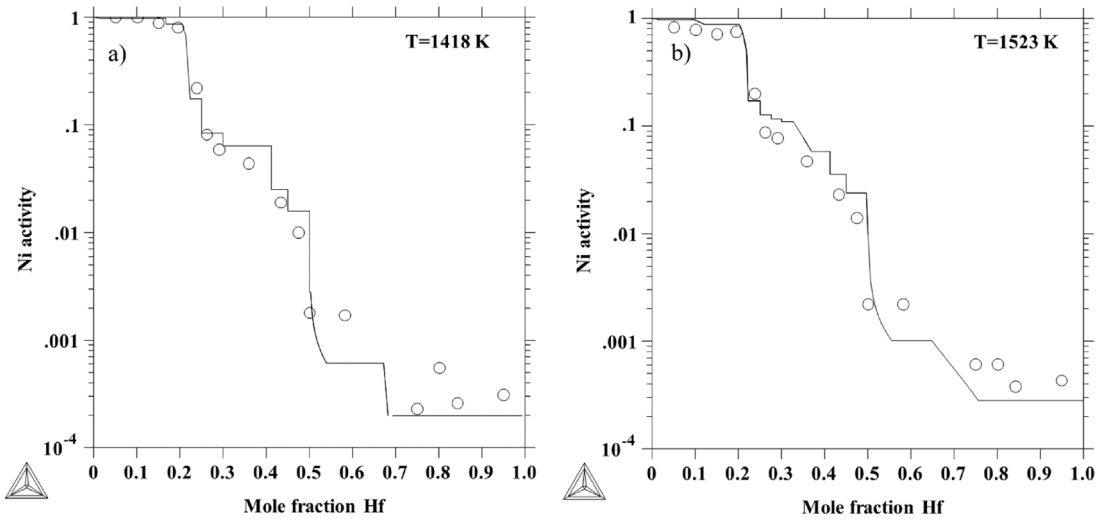

Fig. 5. Calculated Ni activies from this work at 1418 and 1523 K compared to measurements by Bencze [14] (◯) with a Ni reference state of fcc at the given temperature in each case.

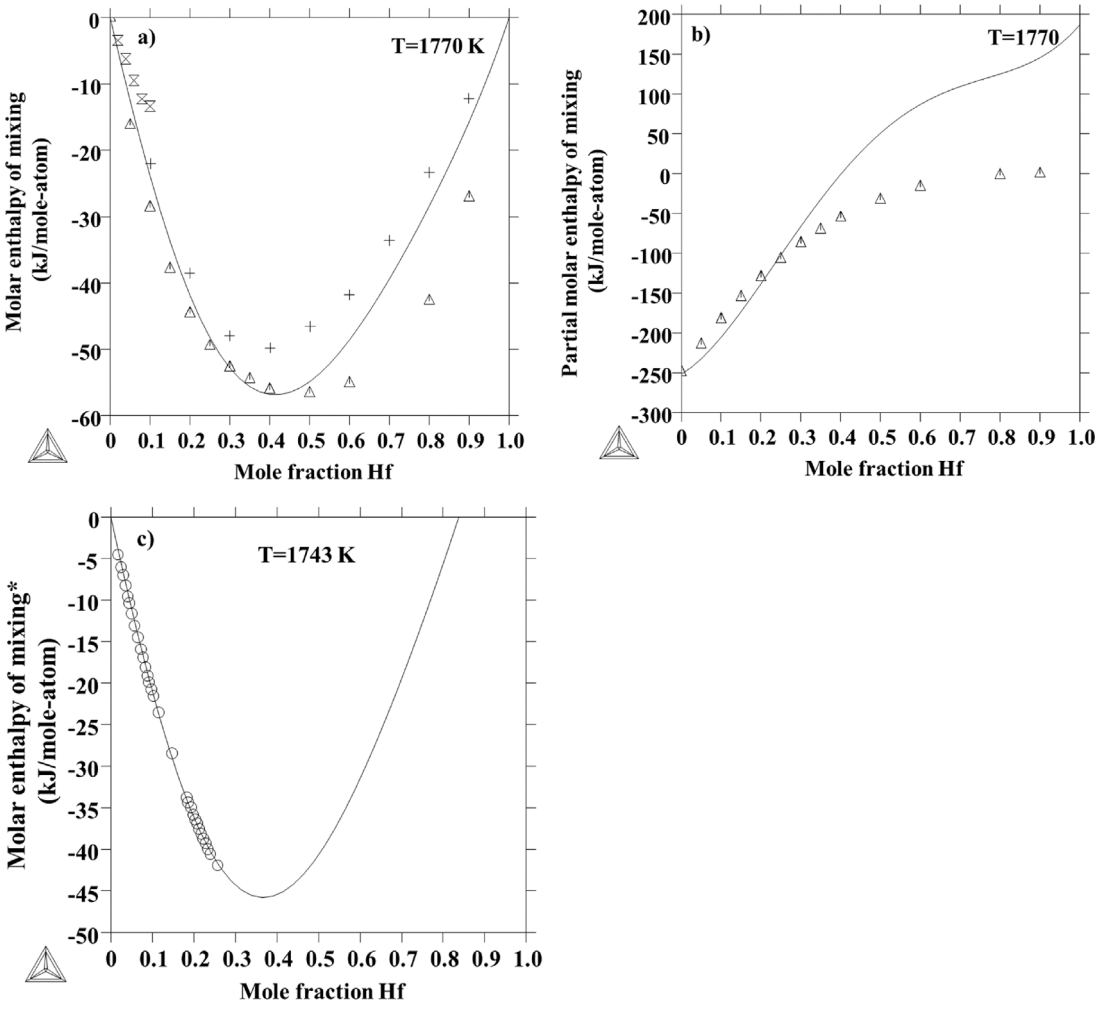

Fig. 6. Thermochemical calculations in the liquid phase: a) the molar enthalpy of mixing at 1770 K compared to experiments by Podoprigora and Sudavtsova [19,20], at 1770 K (△) and Sudavtsova [21] at 1877 K (+) and thesis work cited by Podoprigora and Sudavtsova [19] [20], (⊠) b) calculated partial molar enthalpy of mixing compared to Podoprigora and Sudavtsova at 1770 K [19,20], (△) and c) calculated molar enthalpy of mixing (*with respect to solid hcp Hf and liquid Ni) at 1743 K compared to data by Selhaoui [13] at this temperature (◯).

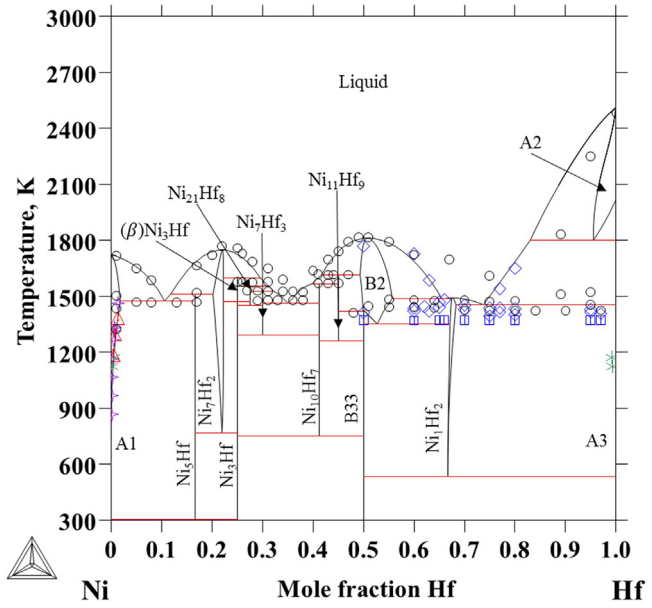

Fig. 7. Hf-Ni phase diagram from 300 to 3000 K plotted with DTA data by Svechnikov et al. [11](○) DTA data, two phase observations, and single phase observations by Yeremenko [18] (◇, ◫, and □ respectively) and solubility measurements by Wang et al. [7] (✳) solubility measurements by Hajjaji et al. [10] (✦) and solubility measurements from this work (△).

achieved to this data. Optimization to the activity represented by the equilibria between B2 and the liquid is not achieved. Agreement is also worse on the Hf-rich portion of the diagram. However, there is a large degree scatter in the experimental values for samples with low Ni activities in this portion.

6.4.2. Thermochemical data in the liquid phase

The enthalpies of mixing at 1770 K, partial enthalpy of mixing at 1770 K, and the enthalpy of mixing with respect to liquid Ni and solid hcp at 1743 K is plotted in Fig. 6a, b and c respectively. The collected mixing enthalpies were fit to during optimization and, hence, the resulting mixing enthalpy is an average of experimental values. Disagreement occurs with higher Hf concentrations between datasets. This is why partial enthalpy calculations by Podoprigora et al. [20] and Sudavtsova et al. [21] disagree with the present model and why experimental partial enthalpies agree well for low Hf concentration in the liquid.

6.4.3. The liquidus and sources of disagreement in this work

The Hf-Ni phase diagram is plotted in Fig. 7. Invariant reactions agree well with the collected experimental invariant reactions with the exception of those between B2 and the NiHf2 phase. The disagreement between DTA from Yeremenko et al. [3] and Svechinkov et al. [11] data is stark with a difference of roughly 200 K between the two experiments near 66 at.% Hf. Work by Eremenko [24] showed that the liquidus between the compounds NiZr and NiHf was roughly a linear interpolation between the melting points of these two compounds: 1543 and 1778 K, respectively. The liquidus surface should not be drastically different between $NiHf_2$ and $NiZr_2$ so of the two datasets, assuming no error between datasets, measurements by Yeremenko et al. [3] are more likely to be contaminated by Zr. However, it was not possible to fit to data by Svechinkov et al. [11] and simultaneously capture the surrounding eutectics. Hence, near the $NiHf_2$ phase, DTA data by only Yeremenko et al. [3] was used to fit the liquidus in this region. The catatectic on the Hf-rich portion was subsequently affected with a calculated value of 1802 K which is much higher than 1428 K suggested by Yeremenko et al. [3]. While it is possible to adjust the liquid energy in this region of the phase diagram to yield an acceptable fit to the measured phase boundaries and catatectic reaction, this would require a more intricate model such as the associate model or the modified quasichemical model [48]. It is the opinion of the authors that more experimental work is needed with high purity samples in the Zr-rich portion before more complex models are implemented.

6.4.4. Hf solubility in fcc Ni and the $L1_2$ phase

The Ni-rich portion of the Hf-Ni phase diagram displaying equilibrium between the fcc solution phase and Ni_7Hf_2 phase from 800 K to 1600 K with experiments from this work and work by Hajjaji [10] and Wang [7] is given in Fig. 8a. The solubility measurements in this work were larger than the solubility measured by Hajjaji [10]. This may be due to the Zr present in the samples but it may also be due the heat treatment by Hajjaji [10] which was not stated. If these heat treatment times were sufficiently small it may be that the experiments did not quite reach equilibrium. Indeed, heat treatments of 1200 and 1440 h by Wang et al. [7] yield solubility measurements close to the present results. Hence, the present fitting was performed only with respect to the experiments in this work.

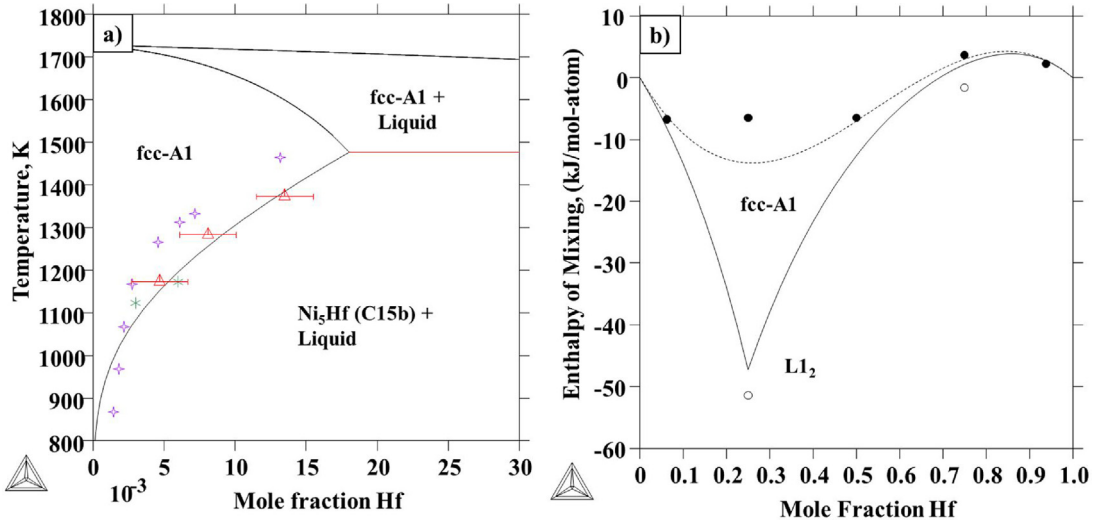

Fig. 8. a) Solubility of Hf in fcc (A1) Ni and b) calculated mixing enthalpy of the fcc A1 phase and the L12 phase resulting from CALPHAD optimization plotted with calculated mixing from first-principles from this work for each phase (● and ○ respectively). Solubility measurements by Wang et al. [7]. (✳) solubility measurements by Hajjaji et al. [10] (✦) and solubility measurements from this work (△).

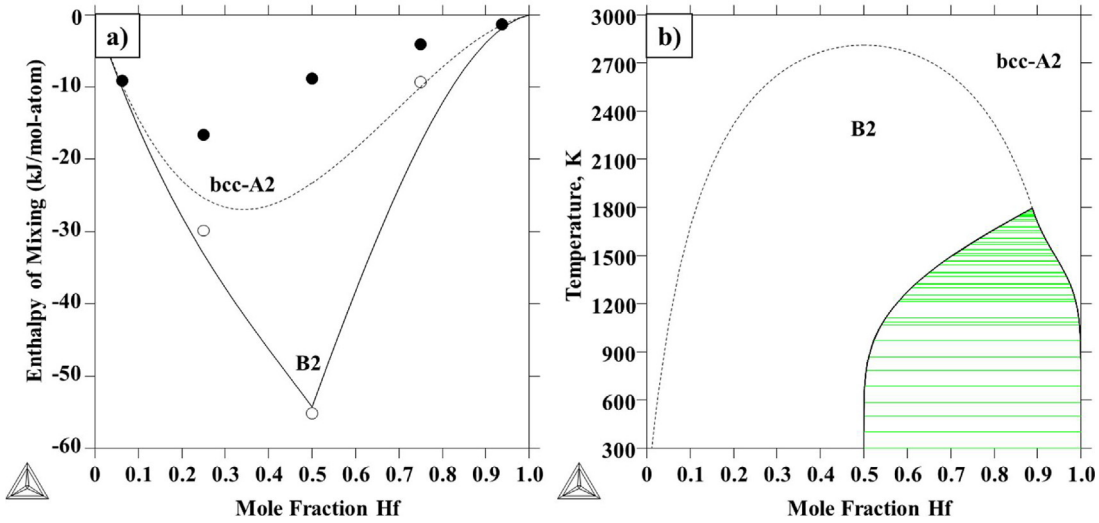

Fig. 9. a) calculated mixing enthalpy of the bcc-A2 phase and the B2 phase resulting from CALPHAD optimization plotted with calculated mixing from first-principles from this work for each phase (● and ○ respectively) and b) the metastable bcc-A2-B2 phase diagram. A dotted line shows the second-order phase transition between bcc-A2 and B2.

The fit to SQS calculations along with the calculated metastable diagram resulting from this paper's fitting is given in Fig. 8b. The asymmetric mixing did not require major modification during solubility fitting and the $L1_2$ enthalpy with respect to the fcc phase was replicated to a reasonable degree without α terms. This asymetric mixing is consistent with the chemically similar Ni-Ti [49] and Ni-Zr [50] models, each of which has a more negative mixing enthalpy on the Ni-rich portion of the diagram.

6.4.5. *The bcc-A2 and B2 phases*

Given the confirmation of the B2 phase by high-temperature synchrotron, the high temperature NiHf phase phase was modeled with this crystal structure with a transition temperature of 1433 K in accordance with DSC and high temperature Synchrotron data. A plot of the phase diagram containing the high temperature B2 phase is given in Fig. 7 from 45 to 75 at.% Hf. The parameters for the B2 phase were adjusted based on the surrounding equilibrium in the system. Good agreement is found with the surrounding transition temperatures and experimental liquidus obtained. Good agreement is also found with DTA data from Svechinkov [11] and from Yeremenko [3] near 50 at.% Hf. However, there are unaccounted transitions in the present description between the NiHf phase and the $NiHf_2$ phase. It is likely that this is caused by a wider solubility range for Ni in this phase at higher temperatures. Since this could not be confirmed it was not addressed further here. The calculated value for the transition from B33 to B2 was 1420 K which falls close to the measured value of 1433 K by DSC and synchrotron data in this work.

A plot of the mixing enthalpies resulting from SQS calculations and the metastable diagram bcc-B2 diagram is given in Fig. 9a and b, respectively. A fit of the bcc mixing enthalpy was not possible simultaneously with the B2 enthalpy with respect to the bcc end-members and the modeled liquidus.

7. Conclusions

A thorough investigation into the nickel-rich portion of the Hf-Ni system is performed using both first-principles calculations and experiments. New experiments are made using HfNi with relatively low Zr contamination (0.25 wt. % Zr in the starting Hf). Diffusion couple experiments are carried out at 1173, 1273, and 1373 K to confirm the phase stability observed in previous experiments and to measure the Hf solubility in fcc Ni. This solubility is of key importance to understanding and predicting the Hf activity in Ni-rich alloys containing Hf as a component to improve the oxidation resistance of the alloy. CALPHAD modeling is carried out using phase stability data from these diffusion couples and from the literature, thermochemical data in the literature and calculated thermochemical data from first-principles calculations. The resulting phase diagram and thermochemical properties agree well with available experiments.

First-principles thermochemical data at 0 K and finite temperatures provided a physical basis for the modeling of experimentally observed phases and unstable phases having the $L1_2$ crystal structure. This description of the $L1_2$ phase in this system is important for extrapolations into higher-order systems. Special quasi-random structures are used to obtain mixing enthalpies in the fcc and B2 systems. The stability of the B2 phase is also important to oxidation resistant alloys given the prominence of the B2-NiAl phase in high-temperature alloys and coatings. The stability is investigated using DSC to confirm the presence of a high temperature phase and high-temperature synchrotron experiments to confirm that the crystal structure of this phase is B2 above the transition temperature. DSC results found a high temperature transition at 1433 K and HEXRD experiments confirmed this phase to be the B2 phase – although the exact nature of the transformation still warrants investigation. This is significant since it represents the first time the B2 phase in the Hf-Ni system has been observed experimentally to the knowledge of the authors. Previously, the B2 phase was only suggested to form a solid solution with the B2-NiTi phase from DSC measurements. However, previous experiments could not directly observe the B2 phase due to symmetry changes caused by quenching in samples rich in Hf. Special quasi-random structures are subsequently used to model the bcc phase and the B2 phase is modeled as a solution phase in tandem with modeling of the bcc phase. The stability range of the B2 phase fit using first-principles will provide important groundwork for future databases built to design shape-memory alloys and high temperature coatings.

Acknowledgments

This work was funded by the U.S. Department of Energy through Grant DE-FE0024056 and DE-FE0031553. First-principles calculations were carried out partially on the LION clusters supported by the Materials Simulation Center and the Research Computing and Cyber infrastructure unit at the Pennsylvania State University, partially on the resources of NERSC supported by the Office of Science of the U.S. DOE

under Contract No. DE-AC02-05CH11231, and partially on the resources of XSEDE supported by National Science Foundation with Grant ACI-1053575.

Appendix A. Supplementary data

Supplementary data associated with this article can be found, in the online version, at https://doi.org/10.1016/j.tca.2018.08.011.

References

[1] P.Y. Hou, Impurity effects on alumina scale growth, J. Am. Ceram. Soc. 86 (April (4)) (2003) 660–668.
[2] G. Firstov, J. Van Humbeeck, Y. Koval, Comparison of high temperature shape memory behaviour for ZrCu-based, Ti–Ni–Zr and Ti–Ni–Hf alloys, Scr. Mater. 50 (January (2)) (2004) 243–248.
[3] V.N. Yeremenko, E.L. Semenova, L.A. Tretyachenko, V.M. Petyukh, Constitution of the Hf-Ni system up to 50 at.% Ni, J. Alloys Compd. 191 (January (1)) (1993) 117–119.
[4] Y. Kim, R. Ashbrook, Directionally Solidified Pseudo-binary Eutectics of Ni-Cr-(Hf, Zr), (1975).
[5] V. Khorunov, V. Ivanchenko, V. Kvasnitskij, Structure and phase composition of Ni-Cr-Zr and Ni-Cr-Hf alloys used as brazing alloys, Avtom. Svarka 11 (1999) 14–22.
[6] A. Berche, J.C. Tédenac, P. Jund, Phase diagram and enthalpy of formation of Hf-Ni-Sn, Comput. Mater. Sci. 125 (December) (2016) 271–277.
[7] T. Wang, Z. Jin, J.-C. Zhao, Experimental study and reassessment of the Ni-Hf binary system, Zeitschrift für Met. 92 (5) (2001) 441–446.
[8] C. Zhang, J. Zhu, Y. Yang, H.-B. Cao, F. Zhang, W.-S. Cao, Y.A. Chang, Thermodynamic modeling and experimental investigation of the Ni-rich corner of the Ni-Al-Hf system, Intermetallics 16 (February (2)) (2008) 139–147.
[9] X. Yang, C. Pin, A. Fane, Separation of hafnium from zirconium by extraction chromatography with liquid anionic exchangers, J. Chromatogr. Sci. 37 (5) (1999) 171–179.
[10] M. Hajjaji, Solid solubility of hafnium in nickel, J. Alloys 274 (1–2) (1998) 185–188.
[11] V.N. Svechnikov, A.K. Shrin, G.P. Dmitriyeva, The Hafnium-Nickel equilibrium diagram, Izv. Akad. Nauk SSSR, Met. 6 (1967) 176–179.
[12] L. Bsenko, The Hf-Ni and Zr-Ni systems in the region 65–80 at.% Ni, J. Less Common Met. 63 (2) (1979) 171–179.
[13] N. Selhaoui, J.C. Gachon, J. Hertz, Enthalpies of formation of some solid hafnium nickel compounds and of the Ni-Rich HfNi liquid by direct reaction calorimetry, Metall. Trans. B 23 (6) (1992) 815–819.
[14] L. Bencze, K. Hilpert, Thermochemistry of the Ni-Hf system—intermetallic phases, Metall. Mater. Trans. A 27 (11) (1996) 3576–3590.
[15] D. Shin, R. Arróyave, Z.-K. Liu, Thermodynamic modeling of the Hf–Si–O system, Calphad 30 (December (4)) (2006) 375–386.
[16] Q. Guo, O.J. Kleppa, Standard enthalpies of formation of Ni3V, Ni3Hf, PdsHf, and Pt3Sc and systematics of AHof for Ni3Me (Me = La, Hf, Ta), Pd3Me (Me), J. Phys. Chem. 99 (March (9)) (1995) 2854–2856.
[17] Q. Guo, O.J. Kleppa, Standard enthalpies of formation of some alloys formed between group IV elements and group VIII elements, determined by high-temperature direct synthesis calorimetry, J. Alloys Compd. 269 (1–2) (1998) 181–186.
[18] V.N. Yeremenko, E.L. Semenova, L.a. Tretyachenko, V.M. Petyukh, Constitution of the Hf-Ni system up to 50 at.% Ni, J. Alloys Compd. 191 (1) (1993) 117–119.
[19] V.V. Sudavtsova, N.V. Podoprigora, M.A. Shevchenko, Thermodynamic properties of Ni-Hf melts, Powder Metall. Met. Ceram. 49 (7–8) (2010) 478–483.
[20] N.V. Podoprigora, V.S. Sudavtsova, Thermodynamic properties of liquid alloys of the Ni-Hf system, Russ. Metall. 2009 (2) (2009) 107–112.
[21] V. Sudavtsova, N. Sharkina, Interaction in liquid alloys of Fe–Hf and Ni–Hf systems, Neorg. Mater 34 (12) (1998) 1459–1460.
[22] G. Kresse, J. Furthmuller, Comput. Mater. Sci. 6 (1996) 15–50.
[23] O. Levy, G.L.W. Hart, S. Curtarolo, Hafnium binary alloys from experiments and first principles, Acta Mater. 58 (8) (2010) 2887–2897.
[24] N.N. Eremenko, E.L. Semenova, L.A. Tret'yachenko, V. Petyukh, Reaction of equiatomic binary compounds in ternary systems formed by group-IV transition metals with nickel, Inorg. Mater. 28 (1992) 923–927.
[25] P. Nash, D.R.F. West, Phase equilibria in Ni-rich region of Ni–Cr–Hf system, Met. Sci. 15 (August) (1981) 347–352.
[26] P. Nash, D.R.F. West, Phase equilibria in Ni-rich region of Ni-AI-Hf system, Met. Sci. 15 (August) (1981) 347–352.
[27] Z.-K. Liu, First-principles calculations and CALPHAD modeling of thermodynamics, J. Phase Equilib. 30 (September) (2009) 517–534.
[28] M. Hillert, Phase Equilibria, Phase Diagrams and Phase Transformations: Their Thermodynamic Basis, (2007).
[29] M. Hillert, The compound energy formalism, J. Alloys Compd. 320 (May (2)) (2001) 161–176.
[30] K. Lee, P. Nash, The Al-Hf-Ni system (Aluminum-Hafnium-Nickel), J. Phase Equilib. (1991).
[31] I. Ansara, N. Dupin, H.L. Lukas, B. Sundman, Thermodynamic assessment of the Al–Ni system, J. Alloys Compd. 247 (January (1–2)) (1997) 20–30.
[32] N. Dupin, I. Ansara, B. Sundman, Thermodynamic re-assessment of the ternary system Al-Cr-Ni, Calphad 25 (June (2)) (2001) 279–298.
[33] I. Ansara, N. Dupin, H.L. Lukas, B. Sundman, Thermodynamic assessment of the Al–Ni system, J. Alloys Compd. 247 (January (1–2)) (1997) 20–30.
[34] N. Dupin, I. Ansara, B. Sundman, Thermodynamic Re-assessment of the ternary system Al-Cr-Ni, Calphad 25 (2) (2001) 279–298.
[35] A. Kusoffsky, N. Dupin, B. Sundman, On the compound energy formalism applied to fcc ordering, Calphad 25 (December (4)) (2001) 549–565.
[36] J.P. Perdew, K. Burke, M. Ernzerhof, Generalized gradient approximation made simple, Phys. Rev. Lett. 77 (October (18)) (1996) 3865–3868.
[37] G. Kresse, M. Marsman, J. Furthmuller, VASP the Guide, http://cms.mpi.univie.ac.at/vasp/vasp/vasp.html, 2016. [Online]. Available: http://cms.mpi.univie.ac.at/vasp/vasp/vasp.html. (Accessed 01 January 2017).
[38] S.L. Shang, Y. Wang, D. Kim, Z.K. Liu, First-principles thermodynamics from phonon and Debye model: application to Ni and Ni3Al, Comput. Mater. Sci. 47 (4) (2010) 1040–1048.
[39] Y. Wang, Z.K. Liu, L.Q. Chen, Thermodynamic properties of Al, Ni, NiAl, and Ni3Al from first-principles calculations, Acta Mater. 52 (9) (2004) 2665–2671.
[40] S. Shang, Y. Wang, Z.-K. Liu, First-principles elastic constants of α- and θ-Al2O3, Appl. Phys. Lett. 90 (March (10)) (2007) 101909.
[41] C. Jiang, C. Wolverton, J. Sofo, L.-Q. Chen, Z.-K. Liu, First-principles study of binary bcc alloys using special quasirandom structures, Phys. Rev. B 69 (June (21)) (2004) 214202.
[42] C. Wolverton, Crystal structure and stability of complex precipitate phases in Al–Cu–Mg–(Si) and Al–Zn–Mg alloys, Acta Mater. 49 (September (16)) (2001) 3129–3142.
[43] C. Jiang, L.-Q. Chen, Z.-K. Liu, First-principles study of constitutional point defects in B2 NiAl using special quasirandom structures, Acta Mater. 53 (May (9)) (2005) 2643–2652.
[44] Materials Preparation Center, Ames Laboratory USDOE, Ames IA, USA.
[45] J.L. Liu, L.L. Zhu, X.M. Huang, G.M. Cai, Z.P. Jin, Investigation of the phase equilibria in Ti-Ni-Hf system using diffusion triples and equilibrated alloys, Calphad 58 (September) (2017) 160–168.
[46] L.A. Bendersky, A. Roytburd, W. Boettinger, Transformation of BCC and B2 High Temperature Phases to HCP and Orthorhombic structures in the Ti-Al-Nb System. Part I: Microstructural Predictions Based on a Subgroup relation between phases, J. Res. Inst. Stand. Technol. 98 (1993) 561–583.
[47] J.-O. Andersson, T. Helander, L. Höglund, P. Shi, B. Sundman, Thermo-Calc & DICTRA, computational tools for materials science, Calphad 26 (June (2)) (2002) 273–312.
[48] A.D. Pelton, S.A. Degterov, G. Eriksson, C. Robelin, Y. Dessureault, The modified quasichemical model I—binary solutions, Metall. Mater. Trans. B 31 (August (4)) (2000) 651–659.
[49] W.J. Zhu, L.I. Duarte, C. Leinenbach, Experimental study and thermodynamic assessment of the Cu–Ni–Ti system, Calphad 47 (December) (2014) 9–22.
[50] N. Wang, C. Li, Z. Du, F. Wang, Experimental study and thermodynamic re-assessment of the Ni–Zr system, Calphad 31 (December (4)) (2007) 413–421.
[51] N. Selhaoui, J.-C. Gachon, J. Hertz, Enthalpies of formation of some solid hafnium nickel compounds and of the Ni-Rich HfNi liquid by direct reaction calorimetry, Metall. Trans. B 23 (December (6)) (1992) 815–819.